ChemComm

Check for updates

Charge detection mass spectrometry on human-amplified fibrils from different synucleinopathies†

Aikaterini Tsirkou,[a] Flora Kaczorowski,[bcd] Mathieu Verdurand, [ID][bcd] Rana Raffoul,[a] Jonathan Pansieri,‡[e] Isabelle Quadrio, [ID][bcd] Fabien Chauveau [ID]*[d] and Rodolphe Antoine [ID]*[a]

Amyloid fibrils are self-assembled mesoscopic protein aggregates, which can accumulate to form deposits or plaques in the brain. *In vitro* amplification of fibrils can be achieved with real-time quaking-induced conversion (RT-QuIC). However, this emerging technique would benefit from a complementary method to assess structural properties of the amplification products. This work demonstrates the feasibility of nanospray-charge-detection-mass-spectrometry (CDMS) performed on α-synuclein (αSyn) fibrils amplified from human brains with Parkinson's disease (PD) or Dementia with Lewy bodies (DLB) and its synergistic combination with RT-QuIC.

Misfolding and aggregation of cerebral endogenous proteins into pathological, termed "amyloid", structures are crucial features in neurodegenerative diseases such as Alzheimer's disease (AD) and PD,[1–3] and are grouped under the umbrella term of proteinopathies. New strategies to understand and

diagnose these proteinopathies are urgently needed as the global burden of cureless dementia is expected to increase by 60% to 75 million people by 2030.[4,5] Whilst the self-assembly of structurally abnormal proteins into so-called "fibrils" was initially described in the prion field (the protein implicated in Creutzfeldt–Jakob disease), amyloid proteins involved in other neurodegenerative proteinopathies have been shown to share this property. In particular, the seeding ability of the pathological isoform (templating interaction with its native isoform) is a crucial step into the formation of amyloid fibrils.[6] It was shown that RT-QuIC assay is a cutting-edge tool to improve the early diagnosis of human prion diseases and this powerful technique is being extended to other proteinopathies.[4]

Indeed, RT-QuIC amplifies *in vitro* minimal quantities of pathologic isoforms of the protein in biologic samples leading to its detectability. To this end, a recombinant protein is used as a substrate, and Thioflavin-T (ThT) is used as fluorescent reporter to monitor the aggregation phase in real-time while intermittent shaking is performed to foster conversion (see Fig. 1).[7–9] In particular, strategies using RT-QuIC have recently been implemented for α-synucleinopathies, which include PD, DLB, and multiple system atrophy (MSA). In the last 5 years, several groups have reported the amplification of misfolded αSyn in brain homogenate (BH) and cerebrospinal fluid (CSF) of DLB and PD patients.[10,11] After these pioneer studies, further developments are needed to standardize the operating procedures and improve the reproducibility of the RT-QuIC method.[12] In particular, extrinsic and intrinsic factors (like micro-environment, stability and purity of the recombinant protein) need to be controlled or optimized in order to increase the robustness of the technique.[13,14] Furthermore, the idea that the different synucleinopathies could result from distinct αSyn "strains" is gaining increasing credit.[15] Indeed, different structures of αSyn between PD and MSA have been isolated,[16] and amplified,[17,18] suggesting that structural fibril polymorphism could represent the biological substrate of subsequent variable properties in neurodegeneration and inflammatory processes.

[a] Univ Lyon, Université Claude Bernard Lyon 1, CNRS, Institut Lumière Matière, F-69622 Lyon, France. E-mail: rodolphe.antoine@univ-lyon1.fr

[b] Laboratory of Neurobiology and Neurogenetics, Department of Biochemistry and Molecular Biology, Lyon University Hospital, 69677 BRON Cedex, France

[c] Center for Memory Resources and Research, Lyon University Hospital, Lyon 1 University, Villeurbanne, France

[d] Univ Lyon, Centre de Recherche en Neurosciences de Lyon, Equipe BIORAN, Inserm U1028 - CNRS UMR5292, Université Claude Bernard Lyon 1, Groupement Hospitalier Est – CERMEP, 69677 BRON Cedex, France. E-mail: chauveau@cermep.fr

[e] Oxford University, Nuffield Department of Clinical Neurosciences, Oxford University, UK

† Electronic supplementary information (ESI) available: Methods, patient's characteristics, CDMS instrumentation and summary of CDMS analysis, CDMS spectra and ThT detection of αSyn seeding activity in CTRL brain homogenate, normalized fluorescence average curves during RT-QuIC for the 3 patients run in quadruplicate. Additional TEM and CDMS measurements on fibrils amplified from distinct synucleinopathies (Parkinson's disease and dementia with Lewy bodies) and correlation between the RT-QuIC ThT fluorescence peak signal and CDMS ion count rate. See DOI: https://doi.org/10.1039/d2cc00200k

‡ Visiting Address: Level 1 Neuropathology, John Radcliffe Hospital, West Wing Oxford OX3, UK.
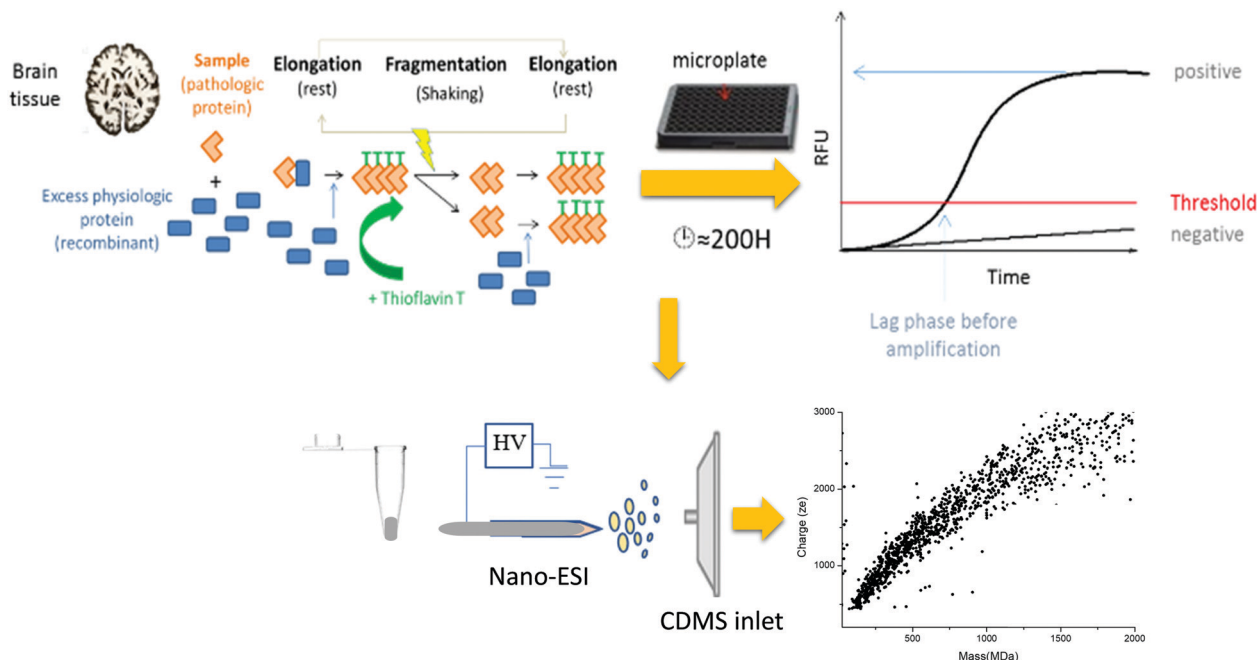
Fig. 1 Schematic representation of the principle of an RT-QuIC reaction followed by a CDMS analysis. Patients' samples (brain homogenates or BH) were added to the reaction mixture containing an excess of physiologic recombinant α-synuclein protein and Thioflavin T (ThT). During the elongation period (rest), and according to the "prion-like" effect, the misfolded pathologic protein contained in the sample transmits its mis-conformation to the recombinant protein forming beta-sheets and integrating the ThT fluorophore into the fibrils in formation. Then, a fragmentation step of "shaking" breaks the fibrils into multiple smaller ones that are able to elongate and further integrate ThT in successive cycles of amplification. Fluorescence is read every cycle in order to follow the amplification of the signal. In addition, a few μL of samples from microplates are extracted in microtubes and injected in a nanospray tip for CDMS analysis (mass and charge map). BH: brain homogenate; RFU: relative fluorescence unit; nano-ESI: nano-electrospray ionization; HV: nano-ESI high voltage.

However, RT-QuIC does not bring molecular information on the amplified fibrils. RT-QuIC results are expressed as relative fluorescence unit (RFU) over time, and are usually interpreted as whether the pathological protein was amplified or not. Hence to date, the structural properties of the amplification products (size, distribution, morphologies of fibrils) have been scarcely studied.[17,19]

Taking into account the large diversity of amyloid forms (oligomers, pre-fibrils, fibrils) and morphologies, complementary techniques analyzing amplification products of RT-QuIC are of high interest. Molecular information such as length distribution is usually estimated by microscopy-derived techniques (Transmission Electronic Microscopy or TEM, Scanning Transmisssion Electronic Microscopy or STEM, Atomic Force Microscopy or AFM).[20–23] However, direct imaging of fibrillar samples is still a challenging and time-consuming method, due to the variations in contrast, the frequent overlap of the fibrils on a 2D matrix, and the limited size of the sample for statistical analyses.[24] Thus, any straightforward and fast complementary technique studying RT-QuIC product fibrillar structures would greatly help in characterizing disease-specific patterns. Recently, we have unequivocally shown the interest of mass measurement of amyloid fibrils by CDMS,[25,26] allowing both the charge and the mass of individual fibrils to be measured within large samples.[27] Besides the determination of mean values, the mass spectrometry-based method performed at the single molecule level allows for recording several

thousands of fibrils in less than one minute leading to the construction of accurate mass and charge distributions. Such distributions can be used to distinguish different species (even weakly populated) present within the sample and their complete characterization (mean values of charge and mass, distribution broadness and population size). These analyses enable an unprecedented characterization of the heterogeneity, polymorphism and co-aggregation between several fibrillar proteins.[28–30] While the interest of using CDMS was demonstrated on synthetic amyloid fibrils, its demonstration for the study of amyloid fibrils from human pathologic materials is lacking. In this study, we propose a synergistic approach bringing together the RT-QuIC strategy with instrumental mass spectrometry based techniques to leverage the characterization of amplified products from BH of pathologically confirmed DLB, PD, and control (CTL) cases (see Fig. 1 for principle schematics). To this end, αSyn in BH was successfully amplified using commercial full-length human αSyn recombinant proteins. A small fraction (2 μL) of the resulting intact material was then submitted to CDMS, which was coupled with a nanospray source (Nanospray Flex Series Ion Source, Thermo-Fisher, see supplemental methods and Fig. S1, ESI†).

Amplification reactions were seeded in quadruplicate for each patient with BH from healthy CTL, PD and DLB patients (see Fig. 2 and Fig. S2, ESI†). After a more than 100 hours elapsed lag-phase, specific amplifications of pathological αSyn were detected from PD and DLB. In Fig. 2, we show selected
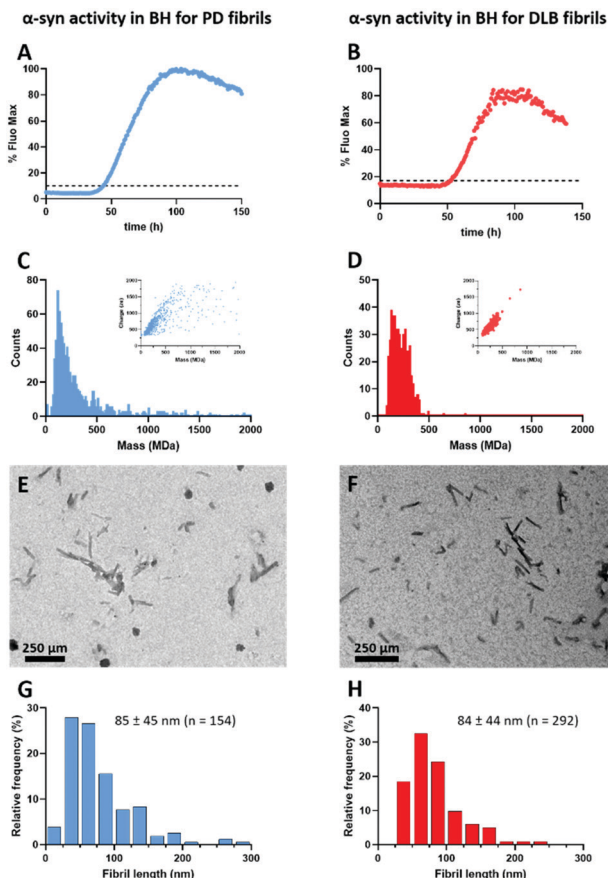
Fig. 2 Results obtained for a single PD (in blue) and single DLB (in red) patients (both amplified with Roboscreen αSyn recombinant protein): ThT detection of αSyn seeding activity in BH (RT-QuIC, panels A and B), and cutoffs shown as a dotted bar (see supplement materials for details, Tables S1 and S2, ESI†), mass distributions of amplified fibrils, with charge vs. mass 2D graphs as inset (CDMS, panels C and D), TEM images of amplified fibrils (panels E and F), and corresponding length distributions (panels G and H).

results obtained for a PD patient (left panels, in blue) and a DLB patient (right panels, in red) amplified with the same recombinant αSyn protein (Roboscreen). Fig. S3 and S4 (ESI†) present other results for a more complete analysis (in particular with amplifications using different recombinant αSyn proteins, from Roboscreen or Rpeptide). Fluorescence intensity signals of ThT peaked around 100 hours and then slowly decreased in both cases, and the maximal fluorescence was slightly higher for PD compared to DLB.

In a separate experiment, BH from a CTL patient led to no or late and non-specific amplification (Fig. S5A–C, ESI†). In CDMS, this control material led to a very weak or no fibril signal (Fig. S5B–D, ESI†). For fibrils showing amplification, a better ion signal was obtained. Among all the different fibril samples examined, a correlation trend was noted between the total fibril ion signal rate recorded by CDMS and the amount of maximal ThT signal after amplification (see Fig. S6, ESI†). For the different synucleinopathies, the 2D graph (charge vs. mass) shown in Fig. 2C and D reported mass measurements on fibrils; m (the mass) of each macroion was obtained from a combination of both

z (the charge) and m/z values. The m and z data are linearly fit. A single slope of that line was observed in the two-dimensional graph (insets in Fig. 2C and D), thus indicating that only one population of fibrils was detected.[29] According to the mass distribution, the mean fibril masses were 170 MDa and 218 MDa with a polydispersity index (PDI) of 1.26 and 1.23 for PD and DLB, respectively (Table S2, ESI†). Clearly, the 2D graph, which was obtained in less than 5 minutes, offered a rapid mass sampling of RT-QuIC fibrillar structures amplified from the tissues of patients with α-synucleinopathies. More importantly, different mean masses were observed for fibrils from PD and DLB RT-QuIC products, which makes the 2D mass-charge graph promising for discriminating the two diseases (and possibly reflecting different αSyn fibril strains).

TEM analysis on amplified samples showed that the average lengths and distributions for PD and DLB fibrils (Fig. 2E–H) are similar. However, CDMS provided a faster and more sensitive technique for discriminating fibril strains, in comparison with the widely-used TEM technique, which required time-consuming procedures and downstream analyses. Indeed, CDMS measures masses instead of lengths on much higher fibril numbers than TEM ($\sim$1000–5000 vs. $\sim$150–300) which provides an important extension to conventional imaging, as mass and charge are more relevant metrics than size for such fibrils in the mesoscopic scale. Further characterization by AFM estimating the height profiles of isolated fibrils might help to better address the mass-charge vs. length relationship.[29]

The highlight of this study is showing how the combination of RT-QuIC and CDMS could be used to examine differences between PD and DLB-derived fibrils. Additional CDMS and TEM measurements were performed on replicates from the same PD and DLB patients and on 3 other patients (two PD and one DLB), and hence a total of 14 (for CDMS) and 10 (for TEM) individual measurements (see Table S3 for details, ESI†) amplified by RT-QuIC (with both Roboscreen and rPeptide αSyn recombinant proteins). We identified various sources of heterogeneity, making it difficult to disentangle the effects of the pathology and the amplification variability (which is highly sensitive to the recombinant protein used, as underlined by the CDMS results, Fig. S3, ESI†). Overall a larger study would be necessary to confirm the observed tendency for DLB to yield longer fibrils than for PD, along with a larger dispersion of mass distribution (Fig. S4, ESI†).

In summary, CDMS has the potential to figure out essential information on the amyloid structures in neuropathology. Its advantages in the field of amyloidosis are further demonstrated through this feasibility report on human-amplified fibrils. CDMS can be conducted with µL containing fibril samples thanks to nanospray ionization coupling. We show that data extracted from CDMS and TEM imaging can be performed on samples amplified by RT-QuIC, allowing multiple perspectives in the comparison of mass, charge and fibril length between different patients with different diseases (polymorphism/ strains) but also within the same disease (intra-population heterogeneity). In addition, more than 5000 fibrils can be analysed by CDMS in less than 5 minutes, allowing for accurate

and representative mass and charge distributions. Altogether, the combination of RT-QuIC, downstream CDMS and conventional imaging may reveal crucial features of amyloid self-assembly in α-synucleinopathies. If further extended to biofluids from living patients (such as cerebrospinal fluid), it might represent a unique opportunity for the early diagnosis and the development of tailored therapies in such cureless diseases.

Conflicts of interest

There are no conflicts to declare.

Notes and references

1 P. Scheltens, B. De Strooper, M. Kivipelto, H. Holstege, G. Chételat, C. E. Teunissen, J. Cummings and W. M. van der Flier, *Lancet*, 2021, **397**, 1577–1590.
2 B. R. Bloem, M. S. Okun and C. Klein, *Lancet*, 2021, **397**, 2284–2303.
3 S. Samanta, M. Ramesh and T. Govindaraju, in *Alzheimer's Disease: Recent Findings in Pathophysiology, Diagnostic and Therapeutic Modalities*, The Royal Society of Chemistry, 2022, pp. 1–34, DOI: 10.1039/9781839162732-00001.
4 S. Singh and M. L. DeMarco, *J. Appl. Lab. Med.*, 2019, **5**, 142–157.
5 C. P. Ferri, M. Prince, C. Brayne, H. Brodaty, L. Fratiglioni, M. Ganguli, K. Hall, K. Hasegawa, H. Hendrie, Y. Huang, A. Jorm, C. Mathers, P. R. Menezes, E. Rimmer and M. Scazufca, *Lancet*, 2005, **366**, 2112–2117.
6 M. Jucker and L. C. Walker, *Nature*, 2013, **501**, 45–51.
7 C. Xue, T. Y. Lin, D. Chang and Z. Guo, *R. Soc. Open Sci.*, 2017, **4**, 160696.
8 K. J. Cao and J. Yang, *Chem. Commun.*, 2018, **54**, 9107–9118.
9 M. Cingolani, L. Mummolo, F. Lugli, M. Zaffagnini and D. Genovese, *New J. Chem.*, 2021, **45**, 14259–14268.
10 G. Fairfoul, L. I. McGuire, S. Pal, J. W. Ironside, J. Neumann, S. Christie, C. Joachim, M. Esiri, S. G. Evetts, M. Rolinski, F. Baig, C. Ruffmann, R. Wade-Martins, M. T. M. Hu, L. Parkkinen and A. J. E. Green, *Ann. Clin. Transl. Neurol.*, 2016, **3**, 812–818.
11 M. Shahnawaz, T. Tokuda, M. Waragai, N. Mendez, R. Ishii, C. Trenkwalder, B. Mollenhauer and C. Soto, *JAMA Neurol.*, 2017, **74**, 163–172.
12 S. Paciotti, G. Bellomo, L. Gatticchi and L. Parnetti, *Front. Neurol.*, 2018, **9**, 415.
13 N. Candelise, M. Schmitz, K. Thüne, M. Cramm, A. Rabano, S. Zafar, E. Stoops, H. Vanderstichele, A. Villar-Pique, F. Llorens and I. Zerr, *Transl. Neurodegener.*, 2020, **9**, 5.
14 K. Sano, R. Atarashi, K. Satoh, D. Ishibashi, T. Nakagaki, Y. Iwasaki, M. Yoshida, S. Murayama, K. Mishima and N. Nishida, *Mol. Neurobiol.*, 2018, **55**, 3916–3930.
15 C. Soto and S. Pritzkow, *Nat. Neurosci.*, 2018, **21**, 1332–1340.
16 T. R. Yamasaki, B. B. Holmes, J. L. Furman, D. D. Dhavale, B. W. Su, E.-S. Song, N. J. Cairns, P. T. Kotzbauer and M. I. Diamond, *J. Biol. Chem.*, 2019, **294**, 1045–1058.
17 M. Shahnawaz, A. Mukherjee, S. Pritzkow, N. Mendez, P. Rabadia, X. Liu, B. Hu, A. Schmeichel, W. Singer, G. Wu, A.-L. Tsai, H. Shirani, K. P. R. Nilsson, P. A. Low and C. Soto, *Nature*, 2020, **578**, 273–277.
18 A. Van der Perren, G. Gelders, A. Fenyi, L. Bousset, F. Brito, W. Peelaerts, C. Van den Haute, S. Gentleman, R. Melki and V. Baekelandt, *Acta Neuropathol.*, 2020, **139**, 977–1000.
19 N. Candelise, M. Schmitz, F. Llorens, A. Villar-Piqué, M. Cramm, T. Thom, S. M. da Silva Correia, J. E. G. da Cunha, W. Möbius, T. F. Outeiro, V. G. Álvarez, M. Banchelli, C. D'Andrea, M. de Angelis, S. Zafar, A. Rabano, P. Matteini and I. Zerr, *Ann. Neurol.*, 2019, **85**, 691–703.
20 S. Guo and B. B. Akhremitchev, *Biomacromolecules*, 2006, **7**, 1630–1636.
21 L. J. Domigan, J. P. Healy, S. J. Meade, R. J. Blaikie and J. A. Gerrard, *Biopolymers*, 2012, **97**, 123–133.
22 D. Oboroceanu, L. Wang, A. Brodkorb, E. Magner and M. A. E. Auty, *J. Agric. Food Chem.*, 2010, **58**, 3667–3673.
23 M. Schmidt, C. Sachse, W. Richter, C. Xu, M. Fändrich and N. Grigorieff, *Proc. Natl. Acad. Sci. U. S. A.*, 2009, **106**, 19813–19818.
24 S. S. Rogers, P. Venema, L. M. C. Sagis, E. van der Linden and A. M. Donald, *Macromolecules*, 2005, **38**, 2948–2958.
25 M. F. Jarrold, *Chem. Rev.*, 2022, **122**, 7415–7441.
26 R. Antoine, *Rapid Commun. Mass Spectrom.*, 2020, **34**, e8539.
27 T. Doussineau, C. Mathevon, L. Altamura, C. Vendrely, P. Dugourd, V. Forge and R. Antoine, *Angew. Chem., Int. Ed.*, 2016, **55**, 2340–2344.
28 R. Bascetin, K. Admane, R. Agniel, T. Boudou, T. Doussineau, R. Antoine, O. Gallet, J. Leroy-Dudal and C. Vendrely, *Int. J. Biol. Macromol.*, 2017, **97**, 733–743.
29 J. Pansieri, M. A. Halim, C. Vendrely, M. Dumoulin, F. Legrand, M. Moulin, S. Chierici, S. Denti, X. Dagany, P. Dugourd, C. Marquette, R. Antoine and V. Forge, *Chem. Sci.*, 2018, **9**, 2791–2796.
30 J. Pansieri, I. A. Iashchishyn, H. Fakhouri, L. Ostojić, M. Malisauskas, G. Musteikyte, V. Smirnovas, M. M. Schneider, T. Scheidt, C. K. Xu, G. Meisl, T. P. J. Knowles, E. Gazit, R. Antoine and L. A. Morozova-Roche, *Chem. Sci.*, 2020, **11**, 7031–7039.